# The Thermodynamic Links between Substrate, Enzyme, and Microbial Dynamics in Michaelis–Menten–Monod Kinetics

FEDERICO MAGGI,[1] FIONA H. M. TANG,[1] WILLIAM J. RILEY[2]

[1]School of Civil Engineering, The University of Sydney, Sydney, 2006, NSW, Australia [2]Earth Sciences Division, Lawrence Berkeley National Laboratory, Berkeley, CA, 94720

Correspondence to: Federico Maggi; e-mail: federico.maggi@sydney.edu.au

ABSTRACT

Accurate prediction of the temperature response of the velocity $v$ of a biochemical reaction has wide applications in cell biology, reaction design, and biomass yield enhancement. Here, we introduce a simple but comprehensive mechanistic approach that uses thermodynamics and biochemical kinetics to describe and link the reaction rate and Michaelis–Menten constants ($k_T$ and $K_T$) with the biomass yield and mortality rate ($Y_T$ and $\delta_T$) as explicit functions of $T$. The temperature control is exerted by catabolic enthalpy at low temperatures and catabolic entropy at high temperatures, whereas changes in cell and enzyme–substrate heat capacity shift the anabolic electron use efficiency $e_A$ and the maximum reaction velocity $v_{max}$. We show that cells have optimal growth when the catabolic (differential) free energy of activation decreases the cell free energy harvest required to duplicate their internal structures as long as electrons for anabolism are available. With the described approach, we accurately predicted observed glucose fermentation and ammonium nitrification dynamics across a wide temperature range with a minimal number of thermodynamics parameters, and we highlight how kinetic parameters are linked to each other using first principles.

INTRODUCTION

Much work has been done to predict how changes in temperature $T$ affect the velocity $v$ of a reaction. The century-old work by van't Hoff and Arrhenius [1], and the later improvements by Eyring's theory of rate processes [2], describe the temperature dependence of chemical reactions, but have recognized limitations. On the one hand, they only describe the temperature dependence of either an equilibrium constant or a reaction rate constant. On the other hand, their monotonic scaling with $T$ cannot describe microbial and enzyme inactivation at low $T$, and cell disruption and enzyme denaturation at high $T$. The Gibbs–Helmholtz formulation relaxes the Gibbs free energy monotonic $T$ scaling and leads to a robust phenomenological

description of enzyme–substrate binding and the maximum reaction rate constant $k$ [3]. For example, cold-adapted enzymes have been shown to lever this mechanism by evolving lower activation enthalpy and more negative activation entropy [4], which were recently explained by a structurally more flexible receiving site in the outermost enzyme portion [5]. Remarkably, changes in activation entropy and enthalpy balance out, suggesting that $T$ away from optimal for microbially synthesized enzymes induces a regularization of activation enthalpy and entropy that partially copes with nonoptimal conditions and yields higher $k$ and higher $v$ as a consequence. This adaptation mechanism may have evolved to make enzymes expression resilient to low- and high-frequency environmental $T$ fluctuations [6]. Also other factors may be invoked to play a substantial role in the way the velocity $v$ of a biochemical reaction responds to changes in $T$. Earlier evidence that the Michaelis–Menten constant $K$ is sensitive to temperature [3, 7-9], and analyses of $^{15}N/^{14}N$ during denitrification [10] and in experimental $NH_4^+$ and $NO_3^-$ uptake by microalgae and bacteria in [11], converge to suggested that Arrhenius' or Eyring's-like scaling may describe $K$ as a function of $T$ in a similar way as they do for the rate constant $k$ [12]. In contrast, discrepancies arise in the interpretation of the biomass yield $Y$ and how this responds to $T$ because various expression exist (e.g., energy and mass yield, carbon use, assimilation, and respiration efficiency, and others) and because the yield may also be strongly correlated to the availability of one or multiple substrates as energy sources, which can determine the energy flow and the associated energy sinks [13, 14].

The overall picture is that a comprehensive understanding of how $T$ governs not only $k$, but all the kinetic parameters that determine $v$, i.e., $K$, $Y$, and cell mortality rate δ, has not had a unified treatment even if those parameters cumulatively have the most significant effects on the reaction velocity $v$. The overarching question is therefore whether it is possible to find a meaningful representation of how the kinetic parameters used in the Michaelis–Menten–Monod (MMM) framework are linked to salient thermodynamic quantities, if they can be expressed as a function of $T$, and whether these can be written in a simple, usable way.

The aim of this work is to introduce and demonstrate application of a novel coupled thermodynamic and kinetic approach that describes how biochemical kinetic parameters ($k$, $K$, $Y$, and $\delta$) share thermodynamic energy and how these relate to $T$. This approach explains temperature dependencies of parameters in microbially mediated reactions and can be generalized to all biochemical reactions that follow MMM kinetics.

MATERIALS AND METHODS

Thermodynamic and Biochemical Aspects of MMM Kinetics

In enzymatic reactions of the MMM type, a substrate $S$ and enzyme $E$ are normally regarded to bind and form an activated complex $C^{\ddagger}$ in equilibrium with $S$ and $E$, which releases the product $P$ and the unchanged enzyme $E$ [15]. Note that the concept of activated complex was not introduced by Michaelis and Menten, but by Eyring while developing the framework transition state within the theory of rate processes. Whereas a number of variant conceptual representations of $E$–$S$ binding exist, including those that account for multiple energy steps [16, 17], this chemical pathway can lead to anabolic growth of the biomass $B$, which synthesizes the enzyme $E$ along the biological pathway [18]. The approach proposed here uses the concepts of near-activation and differential activation (NADA) during complexation at the transition state (Fig. 1a, after [12]). Specifically, NADA identifies two Gibbs free energy levels responsible for an enzymatic reaction to occur; the first is defined by $\Delta G_{NA}^{\ddagger}$ for the near-activation (NA) complexation and the second is $\Delta G_{DA}^{\ddagger} = \lambda \Delta G_{NA}^{\ddagger}$ for differential activation (DA). The two energy levels are associated with the transition state of the complex when a reversible NA equilibrium is reached between reactants and complex ($S + E \rightleftharpoons C \cong C^{\ddagger}$), and when products are irreversibly released ($C \cong C^{\ddagger} \rightarrow P + E$) from the DA complex; NADA differs from earlier approaches in that the two states are separated by the reaction coordinate distance $\delta_a \rightarrow 0$, the characteristic that allows further elaborations. With $\overline{C^{\ddagger}} = (C \cong C^{\ddagger})$, the chemical and biological pathways in NADA biochemical enzymatic reactions can therefore be written as $S + E \underset{k^-}{\overset{k^+}{\rightleftharpoons}} \overline{C^{\ddagger}} \overset{k}{\rightarrow} P + E + YB$ for substrate binding and conversion into products including biomass growth, $B \overset{k_g}{\rightarrow} E + B$ for enzyme production with unchanged biomass, and $B \overset{\delta_B}{\rightarrow} \varnothing$ and $E \overset{\delta_E}{\rightarrow} \varnothing$ for biomass mortality and enzyme degradation. Here, $k^+$ and $k^-$ are the rate constants of the forward and backward

equilibrium reactions, $k$ is the reaction rate constant, $Y$ is the biomass yield coefficient expressing the biomass gain per consumed mass of substrate, $k_E$ is the enzyme synthesis rate, and $\delta_B$ and $\delta_E$ the biomass mortality and enzyme (denaturation) degradation rates, respectively. The corresponding kinetic equations describing the pathways above are

$$\frac{dS}{dt} = -k^+ SE + k^- \overline{C^\ddagger} \quad \text{(1a)}$$

$$\frac{d\overline{C^\ddagger}}{dt} = k^+ SE - k^- \overline{C^\ddagger} - k\overline{C^\ddagger} \quad \text{(1b)}$$

$$\frac{dP}{dt} = k\overline{C^\ddagger} \quad \text{(1c)}$$

$$\frac{dB}{dt} = Y\frac{dP}{dt} - \delta_B B \quad \text{(1d)}$$

$$\frac{dE}{dt} = k_E B - \delta_E E - \frac{d\overline{C^\ddagger}}{dt} \quad \text{(1e)}$$

and can be simplified assuming that $E$ is produced and degrades at rates proportional to the biomass growth and mortality by factor $z$, which expresses the enzyme to biomass ratio. In fact, substituting $k_E B = z(YdP/dt)$ $= z(dB/dt + \delta_B B)$ from Eq. 1d and $\delta_E E = z\delta_B B$ into Eq. 1e, leads to $dE/dt = zdB/dt - d\overline{C^\ddagger}/dt$ [19, 20], and the mass conservation law for $E$ can simply be expressed as $E = zB - \overline{C^\ddagger}$ with $E_0 = zB_0$ and $\overline{C_0^\ddagger} = 0$ at the initial time $t_0$. Using the quasi-steady-state assumption (QSS; [21]) and $E = zB - \overline{C^\ddagger}$ to solve $d\overline{C^\ddagger}/dt = 0$ for $\overline{C^\ddagger}$, leads to

$$\frac{dP}{dt} = kzB\frac{S}{S+K} = -\frac{dS}{dt} \quad \text{(2a)}$$

$$\frac{dB}{dt} = Y\frac{dP}{dt} - \delta_B B = \frac{1}{z}\frac{dE}{dt} \quad \text{(2b)}$$

where $K = (k^- + k)/k^+$ is the Michaelis–Menten constant, and where $dE = zdB$ and $E = zB$ follow from the QSS assumptions $d\overline{C^\ddagger} \approx 0$ and $\overline{C^\ddagger} \approx 0$. It is possible to consider $z$ constant assuming that the enzyme mass fraction in cells is regulated to maintain its level stable; this also implies that $\delta_E \approx \delta_B$.
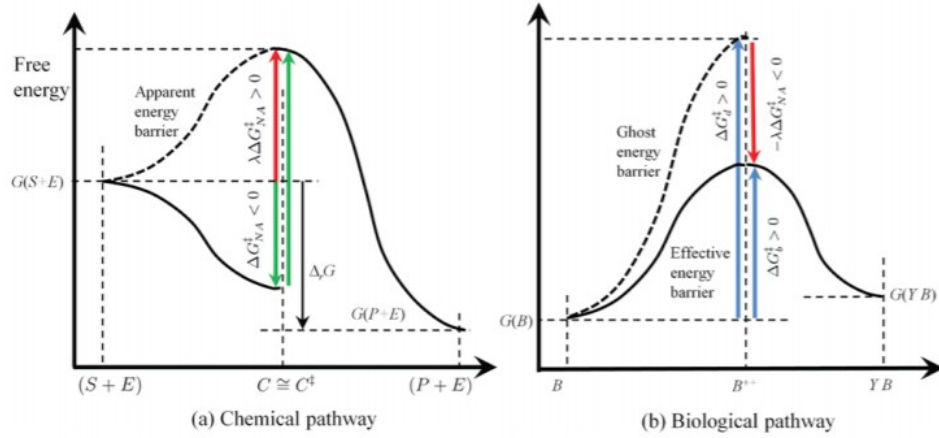
**Figure 1** (a) NADA description of the enzyme–substrate complex binding during the transition state along the reaction coordinate; reversible NA complexation is characterized by Gibbs free energy $\Delta G^{\ddagger}_{NA}$, and irreversible product release is characterized by Gibbs free energy $\Delta G^{\ddagger}_{DA} = \lambda \Delta G^{\ddagger}_{NA}$ with $\lambda < 0$. (b) Biomass Eyring activation process characterized by the Gibbs free energy for cell doubling $\Delta G^{\ddagger}_d$ and the Gibbs free energy for biomass growth $\Delta G^{\ddagger}_b$ along the biomass growth coordinate; the red arrow represents the net apparent energy barrier of the chemical pathway and the corresponding energy detraction in the biological pathway, with the biomass yield $Y$ expressing that growth occurs from one biomass unit to $Y$ units per unit substrate consumption.

Equations (1) and (2) have the same writing as the classical MMM kinetic equations, but they have served to develop the thermodynamic link between $k$ and $K$ in the NADA approach, which is expressed as [12]

$$k = \frac{k_B T}{h}(K^{\ddagger}_{NA})^{\lambda} \quad \text{(3a)}$$

$$K = \frac{1}{K^{\ddagger}_{NA}} + (K^{\ddagger}_{NA})^{\lambda-1} \quad \text{(3b)}$$

where $k_B$ is the Boltzmann constant, $h$ is the Planck constant, and the Boltzmann factor $K^{\ddagger}_{NA} = k^+/k^- = e^{-\Delta G^{\ddagger}_{NA}/RT}$ is the NA complexation constant [12]. Note that the term $K^{\ddagger}_{DA} = (K^{\ddagger}_{NA})^{\lambda}$ for DA corresponds to that in the classical Eyring's theory [22, 23], which scales as that of reversible NA complexation by power $\lambda$ (Fig. 1a).

The NADA kinetic parameters in Eq. (3) also link the biomass yield $Y$ to both $k$ and $K$ as a function of $T$. Using [24], we can demonstrate that the maximum specific biomass growth rate $\mu$ is

$$\mu = zkY \quad \text{(4)}$$

Thus, using Eq. 3a in Eq. 4 leads to

$$Y = \frac{\mu}{z} \frac{h}{k_B T} (K_{NA}^{\ddagger})^{-\lambda} \quad (5)$$

Excluding temperature effects on $z$, which is assumed constant for derivation of Eq. (2), temperature effects in $\mu$ may arise in a form similar to as in $k$, that is, by means of a rate process of the Eyring's type. Using the approach in [25], an activation energy for cell doubling can be hypothesized to consist of a reversible energy capture by cell, and an irreversible transduction into biomass; if substrate concentration effects are excluded, we can define

$$\mu = \frac{k_B T}{h} \cdot K_d^{\ddagger} \quad (6)$$

where the Boltzman factor $K_d^{\ddagger} = e^{-\Delta G_d^{\ddagger}/RT}$ expresses the Gibbs free energy level $\Delta G_d^{\ddagger}$ required by the cell for doubling. Introducing Eq. 6 into Eq. 5 leads to the expression of the temperature-dependent biomass yield

$$Y = \frac{1}{z} K_d^{\ddagger} (K_{NA}^{\ddagger})^{-\lambda} \quad (7)$$

Because the Boltzmann factors $K_d^{\ddagger}$ and $K_{NA}^{\ddagger}$ are exponential functions of Gibbs free energy levels, and because the product of exponential functions is an exponential function, it is possible to define the Gibbs free energy for biomass growth $\Delta G_b^{\ddagger}$ and rewrite Eq. 7 as

$$Y = \frac{1}{z} K_b^{\ddagger} \quad (8)$$

with

$$K_b^{\ddagger} = K_d^{\ddagger} (K_{NA}^{\ddagger})^{-\lambda} = e^{-\Delta G_b^{\ddagger}/RT} \quad (9)$$

where $\Delta G_b^{\ddagger}$ encompasses thermodynamic effects from both $K_{NA}^{\ddagger}$ and $K_d^{\ddagger}$ (Fig. 1b) as

$$\Delta G_b^{\ddagger} = \Delta G_d^{\ddagger} - \lambda \Delta G_{NA}^{\ddagger} \quad (10)$$

Finally, the cell mortality rate $\delta$ has been shown to be a function of $T$ and follows an Arrhenius'-like scaling law in both experiments and modeling exercises [26]. It is therefore meaningful to use a rate process of the Eyring's type also in this case and describe $\delta$ as

$$\delta = \frac{k_B T}{h} K_\delta^{\ddagger} \quad (11)$$

with $K_\delta^\ddagger$ the Boltzmann factor defined by the Gibbs free energy $\Delta G_\delta^\ddagger$ expressing reversible cell inactivation, and with the frequency factor $k_B T/h$ expressing the irreversible cell disruption rate.

The set of temperature-dependent kinetic parameters defining the MMM enzyme kinetics within the NADA approach is therefore

$$k_T = \frac{k_B T}{h}(K_{NA}^\ddagger)^\lambda \tag{12a}$$

$$K_T = \frac{1}{K_{NA}^\ddagger} + (K_{NA}^\ddagger)^{\lambda-1} \tag{12b}$$

$$Y_T = \frac{1}{z}K_d^\ddagger(K_{NA}^\ddagger)^{-\lambda} \tag{12c}$$

$$\delta_T = \frac{k_B T}{h}K_\delta^\ddagger \tag{12d}$$

where subscript $_T$ underlines the explicit accounting of temperature $T$.

Excluding any temperature effects on the Gibbs free energy for mortality in $\Delta G_\delta^\ddagger$ (discussed in detail later), $\Delta G_{NA}^\ddagger$ and $\Delta G_d^\ddagger$ can additionally be decomposed using the Gibbs–Helmholtz enthalpic, entropic, and heat capacity contributions, that is, $\Delta G = \Delta H - T\Delta S$ with

$$\Delta H = \Delta H_0 + \Delta C_p(T - T_0) \tag{13a}$$

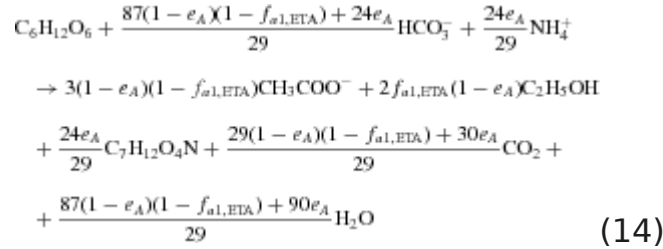$$\Delta S = \Delta S_0 + \Delta C_p \log(T/T_0) \tag{13b}$$

where $\Delta H_0$ and $\Delta S_0$ at the standard temperature $T_0$ have been used in place of other reference $T$, and $\Delta C_p$ is the heat capacity change at constant pressure.

Equations (12) describe the nexus between thermodynamic and kinetic quantities that determine the overall effect of $T$ in a microbial enzyme-mediated reaction.
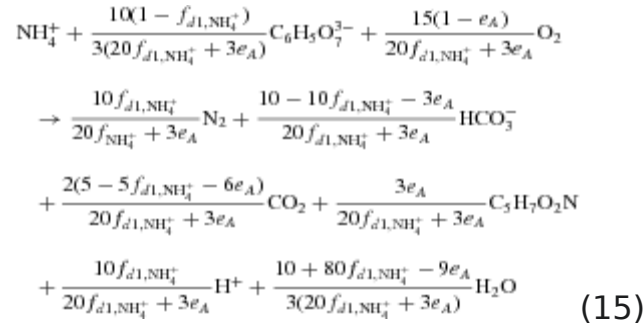
BRIDGING EXPERIMENTS AND MODELING

We tested the temperature-dependent parameters of Eqs. (12) on glucose ($C_6H_{12}O_6$) fermentation to acetate and ethanol by *Brettanomyces bruxellensis* at $T$ between 15 and 32°C [27], and aerobic $NH_4^+$ oxidation by *Alcaligenes faecalis* WY01 in the presence of citrate as the C source at $T$ ranging between 10 and 40°C [28]. Anabolic and catabolic reactions were

used to determine the overall metabolic reactions and stoichiometric coefficients, as well as the relation between $Y_T$ and the fraction $e_A$ of electrons $e^-$ transferred from the catabolic to the anabolic pathway. The two complete reactions are derived with full detail in Supporting Information (SI) Section S1, and writes for $C_6H_{12}O_6$ fermentation as

$$C_6H_{12}O_6 + \frac{87(1-e_A)(1-f_{a1,ETA})+24e_A}{29}HCO_3^- + \frac{24e_A}{29}NH_4^+$$

$$\rightarrow 3(1-e_A)(1-f_{a1,ETA})CH_3COO^- + 2f_{a1,ETA}(1-e_A)C_2H_5OH$$

$$+ \frac{24e_A}{29}C_7H_{12}O_4N + \frac{29(1-e_A)(1-f_{a1,ETA})+30e_A}{29}CO_2 +$$

$$+ \frac{87(1-e_A)(1-f_{a1,ETA})+90e_A}{29}H_2O \tag{14}$$

and for $NH_4^+$ oxidation as

$$NH_4^+ + \frac{10(1-f_{d1,NH_4^+})}{3(20f_{d1,NH_4^+}+3e_A)}C_6H_5O_7^{3-} + \frac{15(1-e_A)}{20f_{d1,NH_4^+}+3e_A}O_2$$

$$\rightarrow \frac{10f_{d1,NH_4^+}}{20f_{NH_4^+}+3e_A}N_2 + \frac{10-10f_{d1,NH_4^+}-3e_A}{20f_{d1,NH_4^+}+3e_A}HCO_3^-$$

$$+ \frac{2(5-5f_{d1,NH_4^+}-6e_A)}{20f_{d1,NH_4^+}+3e_A}CO_2 + \frac{3e_A}{20f_{d1,NH_4^+}+3e_A}C_5H_7O_2N$$

$$+ \frac{10f_{d1,NH_4^+}}{20f_{d1,NH_4^+}+3e_A}H^+ + \frac{10+80f_{d1,NH_4^+}-9e_A}{3(20f_{d1,NH_4^+}+3e_A)}H_2O \tag{15}$$

The corresponding yields $Y*$ in moles of dry mass per mole of consumed substrate are expressed, respectively, as a function of $e_A$ as

$$Y^*_{C_6H_{12}O_6} = \frac{24}{29}e_A \tag{16a}$$

$$Y^*_{NH_4^+} = \frac{3e_A}{20f_{d1,NH_4^+}+3e_A} \tag{16b}$$

with $0 \le e_A \le 1$. Note that the scaling $Y_T \propto Y* \propto \phi(e_A)$, holds in both expressions of $Y*$ in Eq. (16), where $\phi(e_A)$ is a function of $e_A$.

Experimental data relative to $C_6H_{12}O_6$ fermentation and $NH_4^+$ oxidation were divided in two groups for parameter estimation and for model testing using the implicity analytic solution of the MMM problem [20] briefly described in SI Section S2. The unknowns of the chemical pathway ($\lambda$, $\Delta H_{0,NA}^{\ddagger}$, $\Delta S_{0,NA}^{\ddagger}$, and $\Delta C_{p,NA}^{\ddagger}$) and biological pathway ($\Delta H_{0,d}^{\ddagger}$, $\Delta S_{0,d}^{\ddagger}$, $\Delta C_{p,d}^{\ddagger}$, and $\Delta G_{\delta}^{\ddagger}$) were estimated by nonlinear least-square fitting against experimental concentrations,

whereas $z = 10^{-10}$ mol/mg was set constant after [20] assuming that 1% of the microbial biomass was enzyme and that the enzyme molar mass was $10^5$ g mol$^{-1}$ (i.e., 100 kDa = $1.66 \times 10^{-19}$ g per molecule [29]). The standard temperature $T_0 = 25°C$ was used as the reference in the thermodynamic expression of $\Delta G_{NA}^{\ddagger}$ and $\Delta G_d^{\ddagger}$.

## RESULTS

### Experimental Testing

Modeled and experimental concentrations of substrate, product, and biomass relative to $C_6H_{12}O_6$ fermentation and $NH_4^+$ oxidation are represented in Figs. 2 and 3, with the goodness-of-fit expressed by the normalized root mean square error (NRMSE) and correlation coefficient ($R$). With the experimental initial conditions, Eqs. (12) accurately predicted observed dynamics of substrate, products, and biomass over time and all tested $T$. Goodness-of-fit was high on both calibration and independent validation sets for both $C_6H_{12}O_6$ fermentation and $NH_4^+$ oxidation, with no prediction bias in either interpolation or extrapolation $T$ tests.
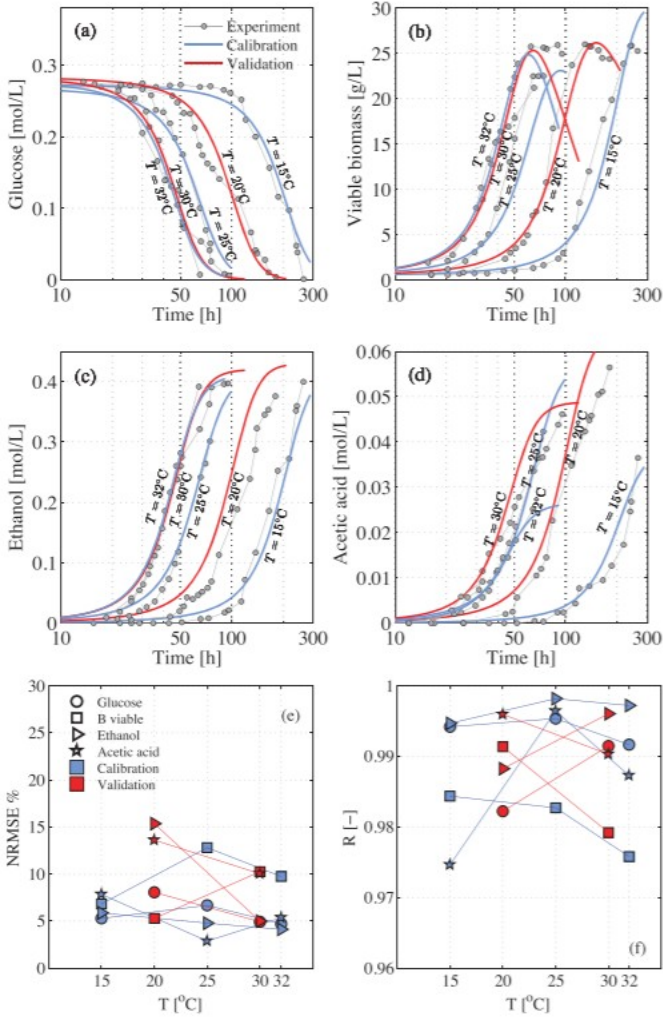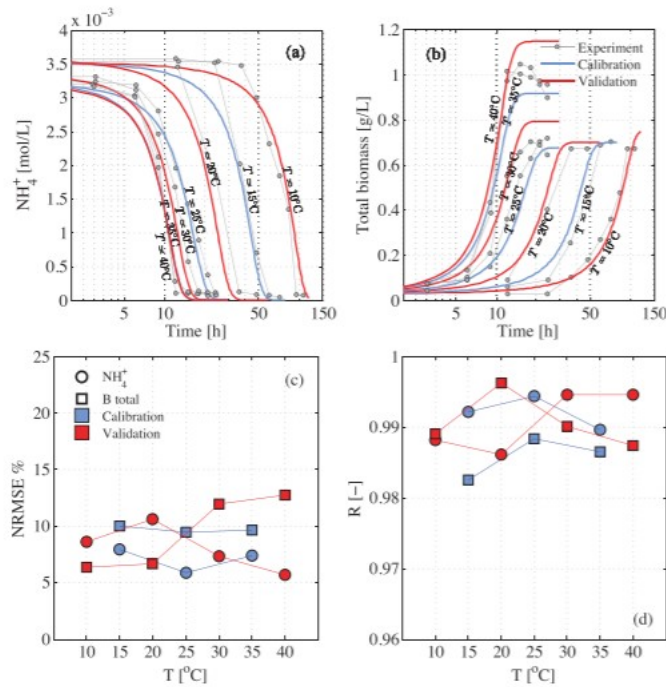
Figure 2. (a)–(d) Experimental and modeled concentrations of substrate (glucose), products (ethanol and acetic acid), and viable biomass over time for $T$ ranging between 15 and 32°C. Experimental data redrawn from [27]. (e)–(f) Goodness of fit expressed by residuals (NRMSE) and correlation coefficient ($R$).

**Figure 3** (a)–(b) Experimental and modeled concentrations of substrate ($NH_4^+$) and total biomass over time for $T$ ranging between 10 and 40°C. Experimental data redrawn from [28]. (c)–(d) Goodness of fit expressed by residuals (NRMSE) and correlation coefficient ($R$).

**Table I** Thermodynamic Parameters for $C_6H_{12}O_6$ Fermentation by B. *bruxellensis* and $NH_4^+$ Oxidation by A. *faecalis*

|   |   |   | $C_6H_{12}O_6$ Fermentation | $NH_4^+$ Oxidation |
|---|---|---|---|---|
| 1 | $\lambda$ |  | −29.73 | −2.87 |
| 2 | $\Delta H_{0,NA}^{\ddagger}$ | (kJ/mol) | −1.62 | −16.69 |
| 3 | $\Delta S_{0,NA}^{\ddagger}$ | (J/mol K) | 2.55 | 30.38 |
| 4 | $\Delta C_{p,NA}^{\ddagger}$ | (kJ/mol K) | 0.30 | 1.97 |
| 5 | $\Delta H_{0,d}^{\ddagger}$ | (kJ/mol) | 62.23 | 61.95 |
| 6 | $\Delta S_{0,d}^{\ddagger}$ | (J/mol K) | −122.83 | −130.20 |
| 7 | $\Delta C_{p,d}^{\ddagger}$ | (kJ/mol K) | −4.31 | −3.66 |
| 8 | $\Delta G_{\delta}^{\ddagger}$ | (kJ/mol) | 110.00 | 110.00 |

## Free Energy in Enzyme–Substrate Binding

The four thermodynamic parameters estimated in the two experimental sets differ by about one order of magnitude but show a consistent trend in their signs (Table I, rows 1–4). Enzyme binding was found to favor the NA complex because the corresponding $K_{NA}^{\ddagger} > 1$ reflects a high enzyme–substrate affinity (Figs. 4a and 4b, light blue curves). Irreversible catabolic product release was characterized by the differential activation factor $K_{DA}^{\ddagger} = (K_{NA}^{\ddagger})^{\lambda} \ll 1$ with $\lambda < 0$ (Figs. 4c and 4d, gray curve). Thus, products released from the DA complex implied the crossing of a relatively high free energy barrier $\Delta G_{DA}^{\ddagger} = \lambda \Delta G_{NA}^{\ddagger} \gg \Delta G_{NA}^{\ddagger}$ (with $\Delta G_{DA}^{\ddagger} = \lambda \Delta G_{NA}^{\ddagger} \gg 0$ and $\Delta G_{NA}^{\ddagger} < 0$) relative to

the energy of inert reactants and NA complex, because $\lambda < -1$ (Figs. 4a–4d, light gray and light blue curves).
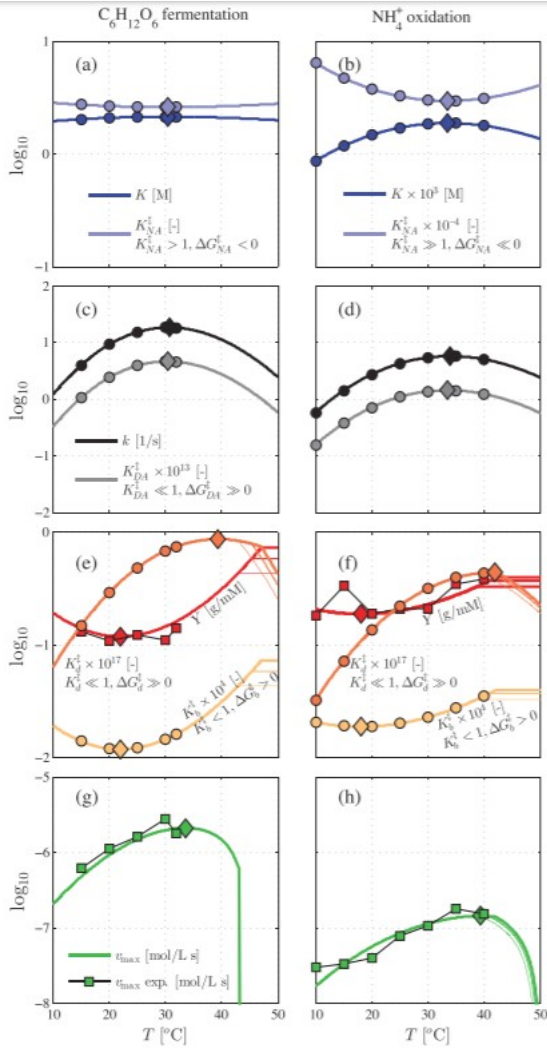


Figure 4. Rows 1–3: temperature-dependent parameters $k_T$, $K_T$, and $Y_T$, and corresponding thermodynamic quantities calculated using Eqs. (12). Row 4: Maximum reaction velocity $v_{max}$ calculated as in SI Section S2. Left and right columns are relative to $C_6H_{12}O_6$ fermentation and $NH_4^+$ oxidation, respectively. Circles are calculated values at experimental $T$. Diamonds indicate calculated maxima or minima. Squares are experimental values.

Values $\Delta C_{p,NA}^{\ddagger} > 0$ (Table I, row 4) signify that the quantity of heat required to raise the NA complex temperature is greater than that of an unbound enzyme and substrate solution at the same concentration if $T$ effects on $C_p$ are excluded [30], whereas negative values $\Delta C_{p,DA}^{\ddagger} = \lambda \Delta C_{p,NA}^{\ddagger} < 0$ for the DA complex signify that the quantity of heat is lower. $\Delta C_{p,NA}^{\ddagger} > 0$ and $\Delta C_{p,DA}^{\ddagger} < 0$ may imply two processes happening at the interface between the enzyme and its binding substrate near and at the active site. On the one hand,

solvent water molecules are rearranged within the enzyme pocket that is about to receive the ligand when the distance between the two shrinks (Fig. 1a). If enzyme binding is hydrophobic, this process also leads to expulsion of some water molecules, which is an enthalpy- rather than entropy-driven process with $\Delta H < 0$ [31]. Hence, excluding entropic effects, a negative $\Delta H$ and the related water expulsion from the active site is suggested to occur and have a substantial effect at temperatures $T < T_0 - \Delta H_{0,NA}^{\ddagger}/\Delta C_{p,NA}^{\ddagger}$ (with $\Delta H_{0,NA}^{\ddagger} < 0$ and $\Delta C_{p,NA}^{\ddagger} > 0$; see derivation in SI Section S3), or disappear at higher temperatures. On the other hand, incorporation of residual interfacial water or ions has been found to result in $\Delta C_P^{\ddagger} < 0$ in some proteins–DNA interfaces [32]. A similar trapping mechanism occurs in $C_6H_{12}O_6$ fermentation and $NH_4^+$ oxidation reactions in Eqs. 15 and 16a, but we found that this mechanism may be reflected in the DA rather than NA complexation because $\Delta C_{p,DA}^{\ddagger} < 0$.

The proposed counterpart thermodynamic explanation to $\Delta C_{p,DA}^{\ddagger} < 0$ is that the DA complex has acquired an amount of Gibbs energy that is in excess of that in the NA complex ($\Delta G_{DA}^{\ddagger} \gg \Delta G_{NA}^{\ddagger}$) and is largely contributed by $\Delta H_{0,DA}^{\ddagger} = \lambda \Delta H_{0,NA}^{\ddagger} \gg \Delta H_{0,NA}^{\ddagger}$ with $\Delta H_{0,DA}^{\ddagger} > 0$ and $\Delta H_{0,NA}^{\ddagger} < 0$ (Table I, row 2). $\Delta C_{p,DA}^{\ddagger} < 0$ indicates therefore the high free energy content of the DA complex and implies that raising its temperature is *easier* than raising the temperature of inert reagents and *much easier* than raising that of the NA complex (Fig. 1a). Changes in structural arrangements at the enzyme–substrate level align with this thermodynamics explanation; in fact, values $\Delta G_{DA}^{\ddagger} \gg 0$ allow for the DA complex to carry out more work than the NA complex, the capability that is encoded into tighter conformational enzyme–substrate bindings as compared to weak NA bindings. These tight bindings can compress the complex active sites (in SI Section S4) and enhance both quantum tunnel and across-energy barrier reactions [33] and are the reasons for lower energy barrier of an enzymatic reaction [34]. Site compression can lead to $\Delta C_{p,DA}^{\ddagger} < 0$, and can limit low-frequency vibrational modes [35]. As suggested in [36], an increased distance between enzyme and substrate implies an increase in binding $T$ dependence, but we have found that this dependence appears to be particularly important in the transient from the NA to DA complex given $\lambda < -1$, that is, $|\Delta C_{p,DA}^{\ddagger}| > |\Delta C_{p,NA}^{\ddagger}|$ ($\Delta C_P^{\ddagger}$ positive for the NA and negative for the DA complex, Table I).

The reason why $\Delta C^{\ddagger}_{p,DA} < 0$ and $\Delta C^{\ddagger}_{p,NA} > 0$ was therefore found in negative $\lambda$ values, which we presume to be a general feature of biochemical reactions.

## Cell Doubling and Biomass Growth

With the description of cell doubling using an Eyring one-step activation process [25], values $K^{\ddagger}_d \ll 1$ correspond to a relatively high-energy barrier $\Delta G^{\ddagger}_d \gg 0$ (Figs. 4e and 4f), which is the free energy that the cell must capture to duplicate internal structures (Fig. 1b). Equation 12c shows that the irreversible DA complex conversion into products expresses an effect on the biomass yield $Y_T$ via the term $(K^{\ddagger}_{NA})^{\lambda}$, and indicates that the free energy eventually required to transduce substrate into biomass is partially sourced in the catabolic pathway (Fig. 1b, red arrow). We have identified two reasons why this mechanism may be effective: The first is that $K^{\ddagger}_{NA} \gg 1$ (Figs. 4a and 4b) and $K^{\ddagger}_d \ll 1$ (Figs. 4e and 4f) facilitate cell reversible free energy harvesting when a strong affinity exists for the enzyme to the substrate; the second is that the net free energy required for biomass growth $\Delta G^{\ddagger}_b$ is lower if $\lambda \Delta G^{\ddagger}_{NA}$ is higher. In fact $\Delta G^{\ddagger}_b = \Delta G^{\ddagger}_d - \lambda \Delta G^{\ddagger}_{NA}$ in Eq. 10 signifies that the catabolic pathway plays a role in the anabolic pathway (Fig. 1b) and also explains why $\Delta C^{\ddagger}_{p,d} < 0$ (Table I, row 7), that is, the amount of free energy stored in the activated cell (metaphase to telophase; Fig. 1b) is higher than in the normal cell. Condition $\Delta G^{\ddagger}_b > 0$ with $\Delta G^{\ddagger}_d > 0$ and $\lambda \Delta G^{\ddagger}_{NA} > 0$, and with the Boltzmann factor for biomass growth being $K^{\ddagger}_b = K^{\ddagger}_d/(K^{\ddagger}_{NA})^{\lambda} < 1$, was met in the two biochemical systems (Figs. 4e and 4f) and is expected to be a general feature as detailed later.

In addition, we demonstrate that $Y_T$, $K^{\ddagger}_b$, and $K^{\ddagger}_d$ must undergo reaction-specific conditions that depend on the $e^-$ fraction used in anabolism; these conditions eventually state that cell doubling and biomass growth can occur upon satisfaction of (see details in SI Section S5)

$$\Delta G^{\ddagger}_d \geq \lambda \Delta G^{\ddagger}_{NA} - RT \ln(z\Phi) \quad (17)$$

$$\Delta G^{\ddagger}_b \geq -RT \ln(z\Phi) \quad (18)$$

with $\Phi = \Phi(m, f_{dry}, e_A, ...)$ a function of various generally known quantities (e.g., biomass stoichiometric composition and molar mass $m$, dry-to-total mass ratio $f_{dry}$, electron fraction used for anabolism $e_A$, etc.).

Using the classification of thermodynamic regions proposed in SI Section S5 and Fig. S2, maps of Eqs. 18 and 19 specific to the two biochemical systems analyzed here show that biomass growth occurred in a thermodynamic island characterized by an energy barrier and no $e^-$ limitation (Fig. 5). In those experiments, $\lambda \Delta G_{NA}^{\ddagger}$ in the chemical pathway was not too high and $e^-$ required for anabolic processes was only a fraction of all $e^-$ extracted from the DA complex (i.e., growth was not limited by $e^-$ and $Y_T$ was relatively low or minimum).
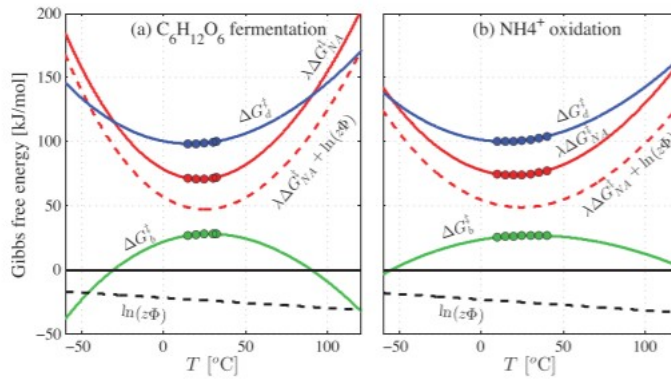


**Figure 5** Free energy of differential activation $\lambda \Delta G_{NA}^{\ddagger}$, cell doubling $\Delta G_{d}^{\ddagger}$, and biomass growth $\Delta G_{b}^{\ddagger}$ as a function of $T$. Markers indicate Gibbs free energy at experimental $T$.

## Cell Survival and Net Biomass Growth

In contrast to $k_T$, $K_T$, and $Y_T$, cell mortality $\delta_T$ may not be the result of an activation process in a strict sense, but of protein denaturation and cell destructuring that increase with an increasing $T$. In describing $\delta_T$ as an Eyring's process via Eq. 12d, the Gibbs free energy $\Delta G_{\delta}^{\ddagger}$ can be interpreted as the energy that a cell has to withhold to survive. The fact that cell survival monotonically decreases with $T$ increasing in contrast to nonmonotonic trends in $k_T$, $K_T$, and $Y_T$, suggests that $\Delta C_{p,\delta}^{\ddagger}$ may have only relatively small effects on $\delta_T$ and can be considered negligible. A value $\Delta G_{p,\delta}^{\ddagger} = 110$ kJ/mol with $\Delta C_{p,\delta}^{\ddagger} = 0$ kJ/mol K was derived from experiments of $C_6H_{12}O_6$ fermentation (which span a timescale long enough to capture mortality) and was used also in $NH_4^+$ oxidation as a proxy, thus $\delta_T$ ranged between about $4 \times 10^{-7}$ and $10^{-5}$ 1/s for $T$ between 10 and 40°C with the prescribed Eyring's scaling.

While the Gibbs free energy of growth $\Delta G_b^{\ddagger}$ and cell mortality $\Delta G_{\delta}^{\ddagger}$ state the potential for the two processes to occur, the actual biomass gain or loss is

determined by combined thermodynamic and kinetic features of the biochemical system. As prescribed by Eq. 3b, the net biomass instantaneous gain is positive or null when $Y_T(-dS/dt) \geq \delta_T B$, or is negative (loss) when $Y_T(-dS/dt) < \delta_T B$. By expanding all thermodynamic terms, net or no biomass gain was verified to occur when (SI Section S6 and Fig. S3)

$$\Delta G_b^\ddagger - \Delta G_\delta^\ddagger \leq -RT \ln \left( z \frac{k_B T}{h} \frac{B}{-dS/dt} \right) \quad (19)$$

Overall, the relationship between $Y_T$ and $k_T$ resulted to be highly nonlinear in both systems, with a sort of loop with vertex at high $k_T$ and low $Y_T$ values at intermediate $T$ (Fig. 6).
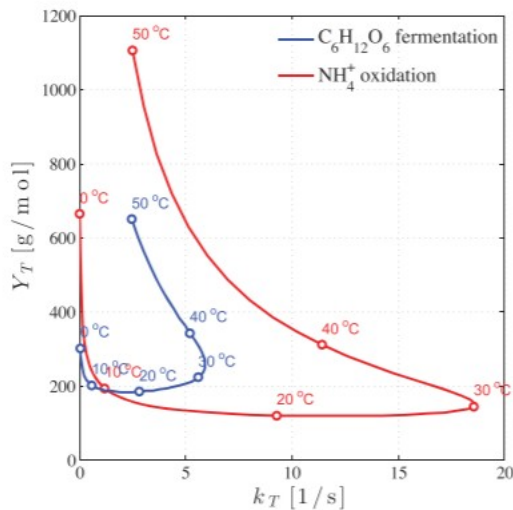


**Figure 6** (a) Relationship between temperature-dependent biomass yield $Y_T$ and reaction rate constant $k_T$.

## Mapping Temperature Patterns

In contrast to intuition, the maximum reaction velocity $v_{max}$ does not necessarily coincide with that of the other kinetic quantities and in particular $k_T$ (Figs. 4d and 4h). A detailed sensitivity mapping of $k_T$, $K_T$, $Y_T$, and $v_{max}$ against $T$ and $\Delta C_{p.DA}^\ddagger$ shows the complexity of interconnections of Eqs. (12) relative to experimental conditions. Regardless of the complete set of gradient isolines (SI Section S7 and Fig. S4), the max $\{k_T\}$, max $\{K_T\}$, and min $\{Y_T\}$ isolines show a general increase in $T$ with an increasing $\Delta C_{p.DA}^\ddagger$ toward $\Delta C_{p.DA}^\ddagger = 0$, when quantities become monotonic with $T$ and follow the Eyring's scaling (Fig. 7). Notably, all $k_T$, $K_T$, and $Y_T$ isolines have an asymptote

at $T_0$ (equal to 25°C in our analyses), the temperature at which any effects of $\Delta C_P^\ddagger$ vanishes. For $\Delta C_{P,DA}^\ddagger < 0$, the dividing line between enthalpy- and entropy-prevalent regimes occurred for $T > T_0$, showing that max $\{k_T\}$, max $\{K_T\}$, and max $\{v_{max}\}$ are prevalently entropy driven, whereas min $\{Y_T\}$ is prevalently enthalpy driven.
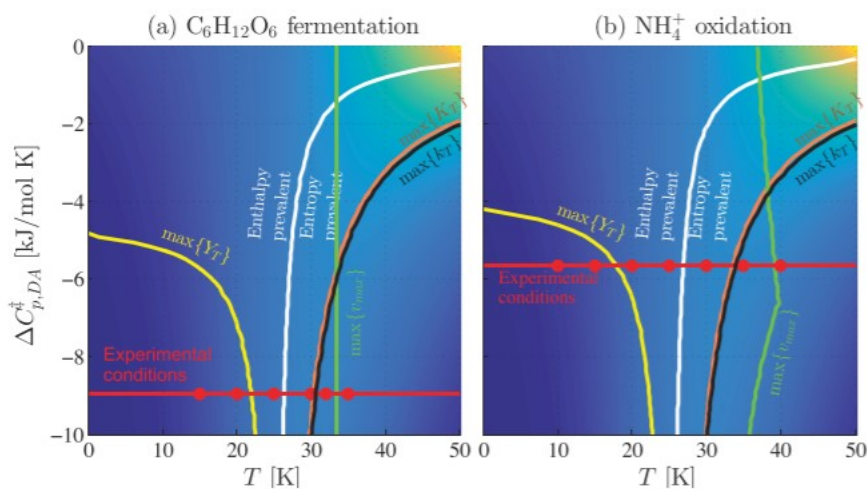


**Figure 7** Maps of temperature-dependent parameters $k_T$, $K_T$, and $Y_T$, and maximum reaction velocity $v_{max}$ as functions of temperature $T$ and heat capacity change $\Delta C_{P,DA}^\ddagger$ of the DA complex. Background color is proportional to $k_T$. Full-detail maps are provided in SI Section S7 and Fig. S4.
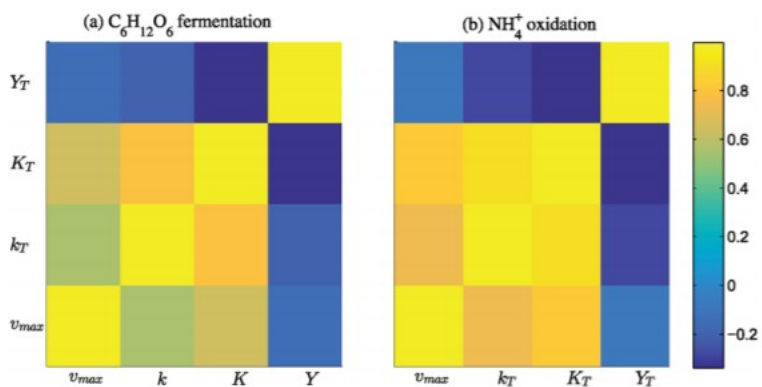


**Figure 8** Combinatorial correlation maps of $k_T$, $K_T$, $Y_T$, and $v_{max}$ calculated from maps in Fig. 7.

These maps show that max $\{k_T\}$, max $\{K_T\}$, and max $\{v_{max}\}$ are nearly concomitant only at a specific $T$ and $\Delta C_{P,DA}^\ddagger$ in both biochemical systems. A more important finding is the close proximity of max $\{k_T\}$ and max $\{K_T\}$, and their relative distance demonstrates that the reaction rate and Michaelis–Menten constants are highly correlated ($R$ about 0.8) regardless of $T$ and $\Delta C_p$ (Fig. 8). Weaker correlations were found across the other temperature-

dependent parameters. In addition, the maximum reaction velocity $v_{max}$ appeared to be more strongly correlated to $K_T$ ($R$ about 0.7) than $k_T$ ($R$ about 0.6) and, more importantly, anticorrelated to $Y_T$ ($R$ about – 0.1).

Mathematical Features

We highlight some mathematical features that Eqs. (12) have, and that can become particularly useful. Equations (12) transform the biochemical system in the classical kinetic parameters ($k$, $K$, $Y$, δ) into the equivalent system of thermodynamic parameters $(\lambda, K_{NA}^{\ddagger}, K_{d}^{\ddagger}, K_{\delta}^{\ddagger})$. The two systems of parameters are reversible, but the latter has the advantage of explicitly accounting for the relationship among kinetic parameters. More importantly, if one wants to retrieve $k$, $K$, $Y$, and δ values from experiments of the same biochemical system at $n$ different temperatures using the same assumptions on $z$ and the QSS approximation, then a total of $4n$ parameters have to be estimated using $n$ systems of $T$-independent MMM kinetic equations. In contrast, Eqs. (12) require eight parameters to describe the same biochemical system at any temperature as long as the thermodynamic parameters can be estimated at two different temperatures at least.

DISCUSSION

Our results show that the free energy levels of the catabolic and anabolic biochemical reaction pathways have a mutual effect on each other; this mutual effect was highlighted in the relationship between $k_T$, $K_T$, and $Y_T$ presented in Eqs. (12). The framework was validated against the biochemistry of $C_6H_{12}O_6$ fermentation and $NH_4^+$ oxidation by different microorganisms at a number of temperatures far from and near the optimal temperature, suggesting that the proposed thermodynamic links embedded in the temperature-dependent parameters provide a robust description of how temperature affects the reaction velocity.

The explicit accounting of $T$ in the tested coupled thermodynamic and kinetic approach has made it possible to map the thermodynamic interconnections between the catabolic and anabolic pathways in biochemical reactions and has led to an explanation to the temperature control and pattern emergence of biochemical reactions that scale down to the way enzyme–substrate

binding occurs, and the way cells canalize free energy and transfer electrons to double their internal structures. Thermodynamic islands for biomass growth have been identified to result from the above mechanisms. Biomass growth has therefore been found to be thermodynamically confined between regions of free energy supply in the catabolic pathway and sink in the anabolic pathway. In particular, we have found that biomass growth does not necessarily occur when the yield is high; in contrast to a general intuition, the (temperature-dependent) yield has a minimum at a certain temperature and increases far from this temperature. At the same time, an increasing distance from optimal temperature reduces the electron transfer efficiency, thus limiting the net biomass gain. In addition, a net biomass gain only occurs when the difference between the Gibbs free energy of biomass growth and mortality satisfies a condition stated by the instantaneous biomass concentration and substrate consumption. The reaction velocity is eventually determined by the overall interplay between Gibbs free energies in the chemical and biological pathways, and the biochemical system state including the biomass dynamics, and not just the reaction rate constant.

In the accounting of the activation process for cell doubling, the simplification introduced in describing cell energy harvesting by means of one reversible process defined by $\triangle G_b^{\ddagger}$ may not capture in full the various stages that mitosis implies. However, following the idea that multiple equilibria in the transition state of enzyme-driven reactions may exist [16, 17], multiple steps in cell activation can be hypothesized with the aim to describe the physiological and genetic processes from the interphase and protophase, to the telophase and cytokinesis, each defined by a Gibbs free energy level. In a sequence of processes of this type, the irreversible segment of cell activation may be identified in the anaphase, when chromosomes are separated and diverted to the two nuclei. This hypothesis may be used to identify how the Gibbs free energy for differential activation in the chemical pathway may affect the various reversible activation steps, and which one of them receives the most important contribution from catabolism. With reference to one-energy level cell activation hypothesis used here, we do however underline that abatement of $\triangle G_b^{\ddagger}$ by $\lambda \Delta G_{NA}^{\ddagger}$ (Fig. 1b) in practice consists of two energy levels, and therefore a type of NADA transition state

may be identified and defined also for biomass growth. This aspect may be the focus of future investigation.

Reactions that are mediated by multiple enzymes, and systems of biochemical reactions that compete for substrates or inhibit each other have not explicitly been investigated in this work. We presume that reactions that involve multiple enzymes sequentially may be described by temperature-dependent kinetic parameters derived as shown in the two cases analyzed here if it is assumed that the energy level in one reaction does not affect those in another reaction. Otherwise, in cases such as competitive and noncompetitive inhibition, or inhibition, the thermodynamic states within NADA and cell doubling may affect each other and, as a consequence, temperature-dependent parameters may also reflect those effects. An incremental extension of the proposed approach to those cases can be attempted and validated as long as experimental data that allow for control are or become available. Examples of biochemical system that can be further used to this purpose are those of catabolite repression [37], [38], where the rate of use of a substrate is favored over another depending on the substrate availability and the capability of a microorganism to sense the substrates and activate the enzyme energetically most convenient to specifically bind to one of them. Catabolite repression has been found to be fundamentally related to enzyme expression and activation, and can be an optimal model system to test temperature effects on multiple enzyme–ligand binding thermodynamics.

CONCLUSIONS

Predicting the velocity $v$ of a biochemical reaction at any arbitrary temperature has been a major target in chemical kinetics, and it still remains a major challenge in biochemistry, where complexity in the chemical and biological pathways couples in a highly nonlinear way. To address this problem, we have developed a coupled thermodynamic and kinetic framework that integrates novel features describing the enzyme–substrate binding at the transition state with the thermodynamics of cell doubling using an Eyring activation approach (Fig. 1). The resulting framework expresses the four key kinetic parameters used to describe MMM reactions as explicit functions of temperature and demonstrates that the temperature-

dependent rate constant $k_T$, the Michaelis–Menten constant $K_T$, and the biomass yield $Y_T$ are correlated with each other because they share the thermodynamics of the enzyme–substrate complex at NA and DA activation. Tests on glucose fermentation and ammonium oxidation provide a strong evidence of the applicability of this approach in the general context of chemical kinetics.

References

1. Atkins, P.; de Paula, J. Physical Chemistry, 8th edn.; W. H. Freeman: Los Angeles, CA, 2006; p. 1053. 2. Glasstone, S.; Laidler, K. J.; Eyring, H. The Theory of Rate Processes; McGraw-Hill: New York, 1941; p. 611. 3. Feller, G. J Phys: Conden Matter 2010, 22(32), 323101. 4. Fields, P. A.; Somero, G. N. PNAS 1998, 95(19), 11476– 11481. 5. Isaksen, G. V.; Aqvist, J.; Brandsdal, B. O. PNAS 2016, 201605237. 6. Stockbridge, R. B.; Lewis, C. A.; Yuan, Y.; Wolfenden, R. PNAS 2010, 107(51), 22102–22105. 7. Fosling, M. L.; Widdas, W. F. J Physiol 1968, 194, 545– 554. 8. Laidler, K. J. The Chemical Kinetics of Enzyme Action; Clarendon: Oxford, UK, 1958; pp. 30–38. 9. Larionova, A. A.; Yevdokimov, I. V.; Bykhovets, S. S. Biogeosciences 2007, 4, 1073–1081. 10. Maggi, F.; Riley, W. J.; 2015, Biogeochemistry, 124, 235–253. DOI: 10.1007/s10533-015-0095-2. 11. Reay, D.; Nedwell, D. B.; Priddle, J.; Ellis-Evans, J. C. Appl Environ Microbiol 1999, 65(6), 2577–2584. 12. Maggi, F.; Riley, W. J. Int J Chem Kinet 2017, 49(5), 305–318. 13. Lipson, D. A. Front Microbiol 2015, 6(615). DOI:10.3389/fmicb.2015.00615. 14. von Stockar, U.; Liu, J. S. Biochim Biophys ActaBioenergetics 1999, 1412(3), 191–211. 15. Laidler, K. J. Can J Chem 1955, 33, 1614–1624. 16. Fersth, A. In Structure and Mechanism in Protein Science; W. H. Freeman: Los Angeles, CA, 1998; Chapter 12. 17. Lienhard, G. E. Science 1973, 180(4082), 149–154. 18.

Rittmann, B. E.; McCarty, P. L. Environmental Biotechnology: Principles and Applications; McGraw-Hill: New York, 2001; p. 754. 19. Maggi, F.; Riley, W. J. Geochim Cosmochim Acta 2010, 74, 1823. 20. Maggi, F.; la Cecilia, D. ACS Omega 2016, 1(5), 894– 898. 21. Briggs, G. E.; Haldane, J. B. S. Biochem J. 1925, 19(2), 338–339. 22. Eyring, H. Chem Rev 1935, 17(1), 65–77. 23. Eyring, H. J Chem Phys 1935, 3(2), 107–115. 24. Bekins, B. A.; Warren, E.; Godsy, E. M. Groundwater 1998, 36(2), 261–268. 25. Desmond-Le Quem´ ener, E.; Bouchez, T. ISME J 2014, ´ 8(8), 1747–1751. 26. Auer, M. T.; Niehaus, S. L. Water Res 1993, 27(4), 693– 701. 27. Brandam, C.; Castro-Mart´ınez, C.; Delia, M. L.; Ram ´ on- ´ Portugal, F.; Strehaiano, P. Can J Microbiol 2007, 54(1), 11–18. 28. Wang, Y.; Chen, H.; Liu, Y.-X.; Ren, R.-P.; Lv, Y.-K. RSC Adv 2015, 5, 79988. DOI: 10.1039/c5ra13318a. 29. Ribbe, M.; Gadkari, D.; Meyer, O. Biol Chem 1997, 272(42), 26627–26633. 30. Privalov, P. L.; Gill, S. J. Adv Protein Chem 1988, 39, 191–234. 31. Hummer, G. Nat Chem 2010, 2(11), 906. 32. Bergqvist, S.; Williams, M. A.; O'Brien, R.; Ladbury, J. E. J Mol Biol 2004, 336(4), 829–842. 33. Hay, S.; Scrutton, N. S. Nat Chem 2012, 4(3), 161–168. 34. Wolfenden, R.; Snider, M. J. Acc Chem Res 2001, 34, 938–945. 35. Arcus, V. L.; Prentice, E. J.; Hobbs, J. K.; Mulholland, A. J.; Van der Kamp, M. W.; Pudney, C. R.; Parker, E. J.; Schipper, L. A. Biochemistry 2016, 55(12), 1681– 1688. 36. Klinman, J. P. Nat Chem 2010, 2(11), 907– 909. 37. Dijkhuizen, L.; van der Werf, B.; Harder, W. Arch Microbiol 1980, 124(2-3), 261–268. 38. Mukherjee, A.; Ghosh, S. J Bacteriol 1987, 169(9), 4361–4367.